Effect of as-solidified microstructure on subsequent solution-treatment process for A356 Al alloy

Bo DANG, Cong-cong LIU, Feng LIU, Ying-zhuo LIU, Yuan-bing LI

State Key Laboratory of Solidification Processing, Northwestern Polytechnical University, Xi'an 710072, China

Abstract: For the compromise of mechanical properties and product cost, the end-chilled sand casting technique was applied to studying the microstructure evolution of A356 Al alloy with cooling rate and the effect of different as-cast microstructures on the subsequent solution-treatment process. The experimental results show that the secondary dendrite arm spacing (SDAS) of primary α(Al), the size of eutectic Si and the volume fraction of Al−Si eutectic are reduced with increasing the cooling rate. Eutectic Si, subjected to solution treatment at 540 °C for 1 h followed by water quenching to room temperature, is completely spheroidized at cooling rate of 2.6 K/s; is partially spheroidized at cooling rate of 0.6 K/s; and is only edge-rounded at cooling rates of 0.22 and 0.12 K /s. Whilst the microhardness is also the maximum at cooling rate of 2.6 K/s. It consequently suggests that subjected to modification by high cooling rate, the eutectic Si is more readily modified, thus shortening the necessary solution time at given solution temperature, i.e., reducing the product cost.

Key words: A356 Al alloy; solution heat treatment; cooling rate; eutectic silicon; modification

1 Introduction

A356 Al alloy has been widely used in automotive industry as material for wheel hub. In order to achieve required mechanical properties, this alloy is often subjected to the heat treatment process, which mainly includes solution treatment process followed by rapidly quenching and aging process [1]. However, the heat treatment on Al alloys is a time and energy consuming process. The high energy cost and competitiveness in the automotive market have forced the industry to redesign the procedure to reduce the product costs.

Upon solution treatment process for Al−Si−Mg alloys, the alloying elements are dissolved into Al matrix to form a supersaturated solid solution in aid of quenching techniques, which then precipitate from the Al matrix in the form of G.P. zones, β'', β' and β, depending on aging temperature and time to harden the alloys [2]. Meanwhile, the eutectic Si is modified by many methods to improve the ductility property of alloys. However, it was reported that the solidified coarse Mg_2Si is completely dissolved at 540 °C within 0.5 h [3], but the

perfect modification of coarse Si particles needs much time. Accordingly, much work of eutectic Si modification was performed. Additions such as Sr [4] and rare earth elements [5] have been used to modify the eutectic Si morphology, namely chemical modification. SAMUEL et al [6] used mischmetal together with cooling rate to modify eutectic Si. Whereas, these trace additions in the rang of 0.1%−6% (mass fraction) are not only difficult to control in practice, but make the metallurgical process too complex to precisely analysis, even producing the porosity defects, thus reducing the mechanical properties [7]. Therefore, a novel approach to modify eutectic Si well in short time, without declining the mechanical properties, is inevitable, but still not available.

The cooling rate, as an important solidification parameter, can significantly modify eutectic Si morphology, i.e., quenching modification, and eliminate some detrimental effect of the impurity intermetallic compound induced in solidification process. Several studies [6,8] were carried out to investigate the microstructure evolution as a function of cooling rate. However, the available results, especially for the

mechanical properties, are sometimes scarcely comparable, since the experiment conditions are not always consistent. For instance, CHEN et al [9] suggested that the liquid melt temperature can influence the subsequent solidification microstructure. Whilst XU and JIANG [10] suggested that the pouring temperature can significantly alter the eutectic Si morphology. Therefore, to create a uniform experimental condition but cooling rate, the end-chilled plate casting was used for the solidification of A356 Al alloy to obtain different solidification microstructures due to different cooling rates, further to study the Si morphology evolution as a function of cooling rate and the effect of variation of solidified Si morphology on solution treatment process, and to simply stress the effect of post-solidification heat on eutectic Si. Finally and importantly, a combination of solidification with solution heat treatment is suggested to efficiently modify the eutectic Si morphology to increase the mechanical properties of alloys with the minimum product cost.

2 Experimental

A356 Al alloy, whose composition is given in Table 1, was melted in a graphite crucible by the electrical resistance furnace. The liquid melt was held at 750 ℃ for 30 min, and then degassed with carbon trichloride shielded by inert gas at 750 ℃. Subjected to two cycles of degassing process, the liquid melt was held at 720 ℃ for 15 min, and then poured into the sand mould to obtain the sample with a shape shown in Fig. 1. It is noted that the chemical modification process was not applied in order to avoid potential contaminant, and all additions and melting handing tools were cleaned with ethanol and coated with daugh along their surface before operation. After casting, the samples were prepared from

Table 1 Composition of A356 Al alloy (mass fraction, %)

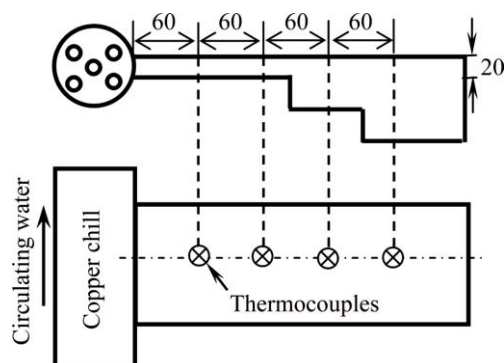| Si	Mg	Fe	Zn	Al
7.4	0.38	0.09	0.01	Bal.

Fig. 1 Schematic diagram of end-chilled plate casting of A356 Al alloy (unit: mm)
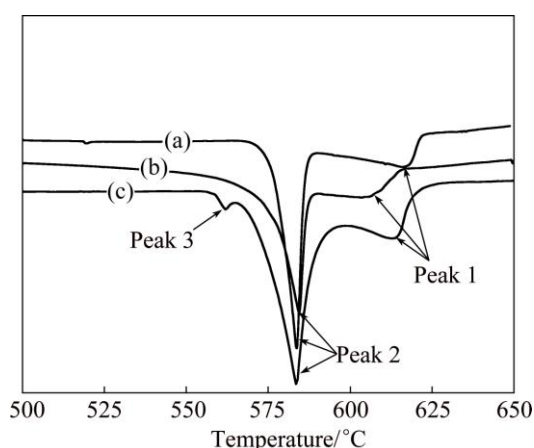
the cast step-like plate perpendicular to copper chill direction. All as-cast samples were treated with a same T4 process, i.e., the samples were held at 540 ℃ for 1 h and then quenched by water bath to room temperature followed by 24 h natural aging.

The K-type thermocouples were used to examine the cooling curve upon solidification, and the relevant data were recorded by an LU−R3000 color paperless recorder. Differential scanning calorimetry (DSC) was performed using a NETZSCH STA 409 PC/PG to determine the phase transforming sequence, the corresponding temperatures, the appropriate pouring temperature in casting process and the maximum of the solution temperature. In the DSC experiment, 20 mg disc-like sample was prepared, and the heating rate of 0.16 K/s and argon flux of 70 mL/min were set. The metallographic samples were etched in 0.5% HF for 30 s after mechanically ground and polished procedures to reveal microstructure morphologies. X-ray diffraction (XRD) combined with energy-dispersive spectroscopy (EDS) was utilized to identify the micro-constituents. Optical microscopy (OM) and scanning electron microscopy (SEM) were used to characterize the as-cast microstructures. Microstructural quantitative analysis was performed on the deeply etched samples using the software IMAGE J. Each sample was measured repetitively by 20 times, and then the mean value was selected.

Microhardness tests were performed using Vickers method (SHIMADZY, Japan). The indentation was made on the well-polished surface of specimens with a diamond square-based pyramid under a load of 9.8 mN for 15 s. The measurements were repeated 10 times and the mean value was calculated.

3 Results

3.1 Solidification behavior

The DSC curves corresponding to the melting of A356 Al alloy cast at different cooling rates (R) are shown in Fig. 2. Two endothermic peaks occur at cooling rates of 2.6 and 0.6 K/s, but an additional small peak occurs at cooling rate of 0.12 K/s, implying that the microstructure constitution depends on the cooling rate. From Ref. [11], the peaks 1, 2 and 3 at about 620, 580 and 554 ℃ in Fig. 2 are relevant to the transformation of primary α(Al) dendrite, Al−Si eutectic and Al+Si+Mg$_2$Si ternary eutectic, respectively. Accordingly, the solidification sequence of A356 Al alloy can be described as: $L \rightarrow \alpha$(Al) dendrite phase $\rightarrow$ Al+Si binary eutectic $\rightarrow$ Al+Si+Mg$_2$Si ternary eutectic.

For the solidification of A356 Al alloy, the cooling curves shown in Fig. 3 were measured by the K-type thermocouples, whose positions in sand mould are shown

Fig. 2 DSC curves of A356 Al alloy with different cooling rates: (a) 2.6 K/s; (b) 0.6 K/s; (c) 0.12 K/s
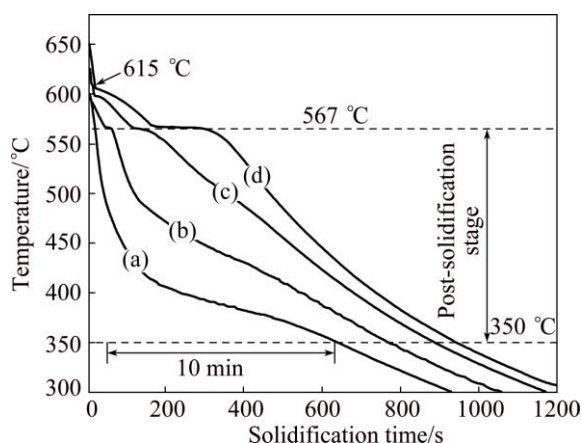

Fig. 3 Cooling curves of end-chill casting with different cooling rates: (a) 2.6 K/s; (b) 0.6 K/s; (c) 0.22 K/s; (d) 0.12 K/s (Post-solidification stage is the temperature range of 350−567 ℃ and the solidification time of curve (a) is 10 min)

in Fig. 1. Obviously, each of cooling curves contains an inflexion and a plateau. From the DSC results (Fig. 2), the inflexion and plateau occurring at ~615 (T_l) and ~567 ℃ (T_e) are associated with the transformation of primary α(Al) dendrite and Al+Si binary eutectic, respectively, implying an identical and reliable experimental condition. However, the ternary eutectic transformation ($L \rightarrow$ Al+Si+Mg$_2$Si), i.e., peak 3, on the DSC curve cannot be observed in Fig. 3, because less Al+Si+Mg$_2$Si ternary eutectic releases the trivial latent heat beyond the K-type thermocouple measurement range. The existed small amounts of Al+Si+Mg$_2$Si ternary eutectic do not significantly influence the experimental analysis result.

3.2 Identification of phases

The micro-constitutions of samples cast at cooling rates of 2.6 and 0.12 K/s were identified by XRD (Fig. 4), where, both the as-cast microstructures are mainly composed of Al phase and Si phase. With increasing the cooling rate, the diffraction angles slightly shift toward higher values, and the half-width of diffraction peaks becomes slightly larger, implying an increased dissolubility of Si and Mg atoms in the Al matrix due to the solute entrapping effect induced by the increased cooling rate [12]. Furthermore, a few of Mg- and Fe-containing intermetallic phases are examined by EDS except for Al phase and Si phase. It is found that the Fe-containing phase presents β-Al$_5$FeSi at high cooling rate and π-Al$_9$FeMg$_3$Si at low cooling rate (Fig. 5) [13]. Accordingly, the solidification microstructures of A356 Al alloy are mainly composed of primary α(Al) phase, Al−Si eutectic and a few Mg- and Fe-containing intermetallic compounds.
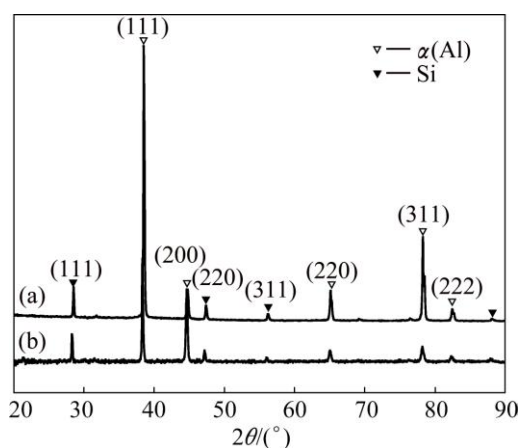

Fig. 4 XRD patterns of A356 Al alloys cast at 2.6 K/s (a) and 0.12 K/s (b)

3.3 Metallurgical characteristics of samples cast at different cooling rates

The metallurgical characteristics of samples cast at four different cooling rates are illustrated in Fig. 5, where, for all the samples, α(Al) dendrite and the coarse plate-like eutectic Si distributed within the interdendritic network are readily identified. In order to further characterize the microstructures, the secondary dendrite arm spacing (SDAS) of primary α(Al) as a function of cooling rate and solidification time, and the shape-factor parameters of eutectic Si as a function of cooling rate were analyzed, respectively.

As shown in Fig. 6(a), the SDAS decreases from ~68 to ~25 μm with increasing the cooling rate from 0.12 to 2.6 K/s. Based on the inverse relationship between the solidification time (t_f) and R, the measured SDAS can be predicted by an empirical equation related to t_f [14,15]:

$$\lambda_2 = 10.23 t_f^{0.33} \tag{1}$$

where λ_2 is the SDAS and t_f is the solidification time. The empirical Eq. (1) offers a considerably precise approach to predict the variation of SDAS as a function
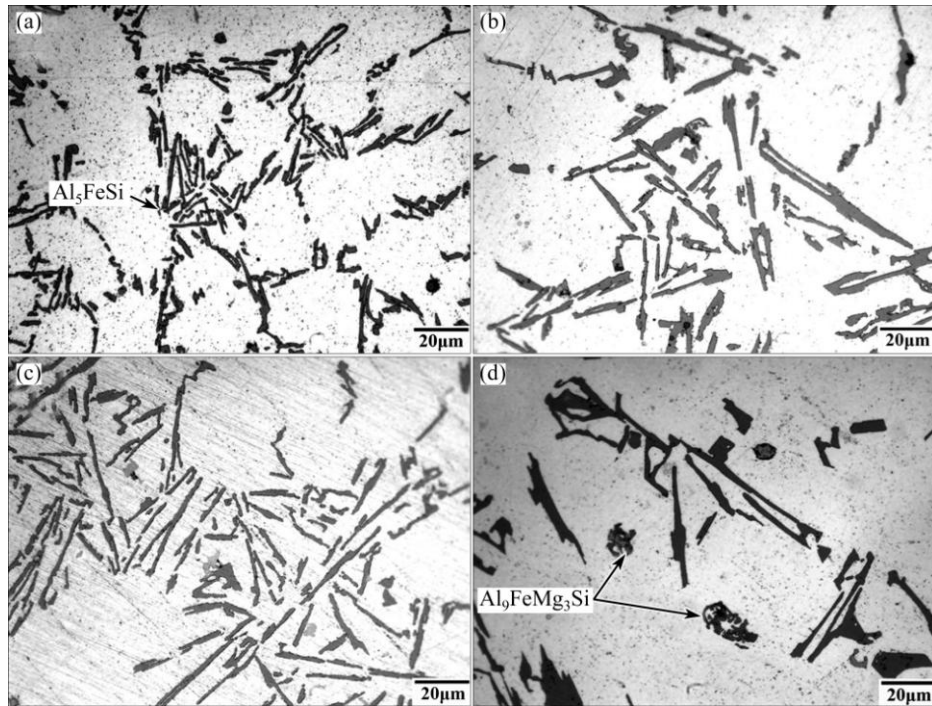
Fig. 5 Microstructures of A356 Al alloys at different cooling rates: (a) 2.6 K/s; (b) 0.6 K/s; (c) 0.22 K/s; (d) 0.12 K/s
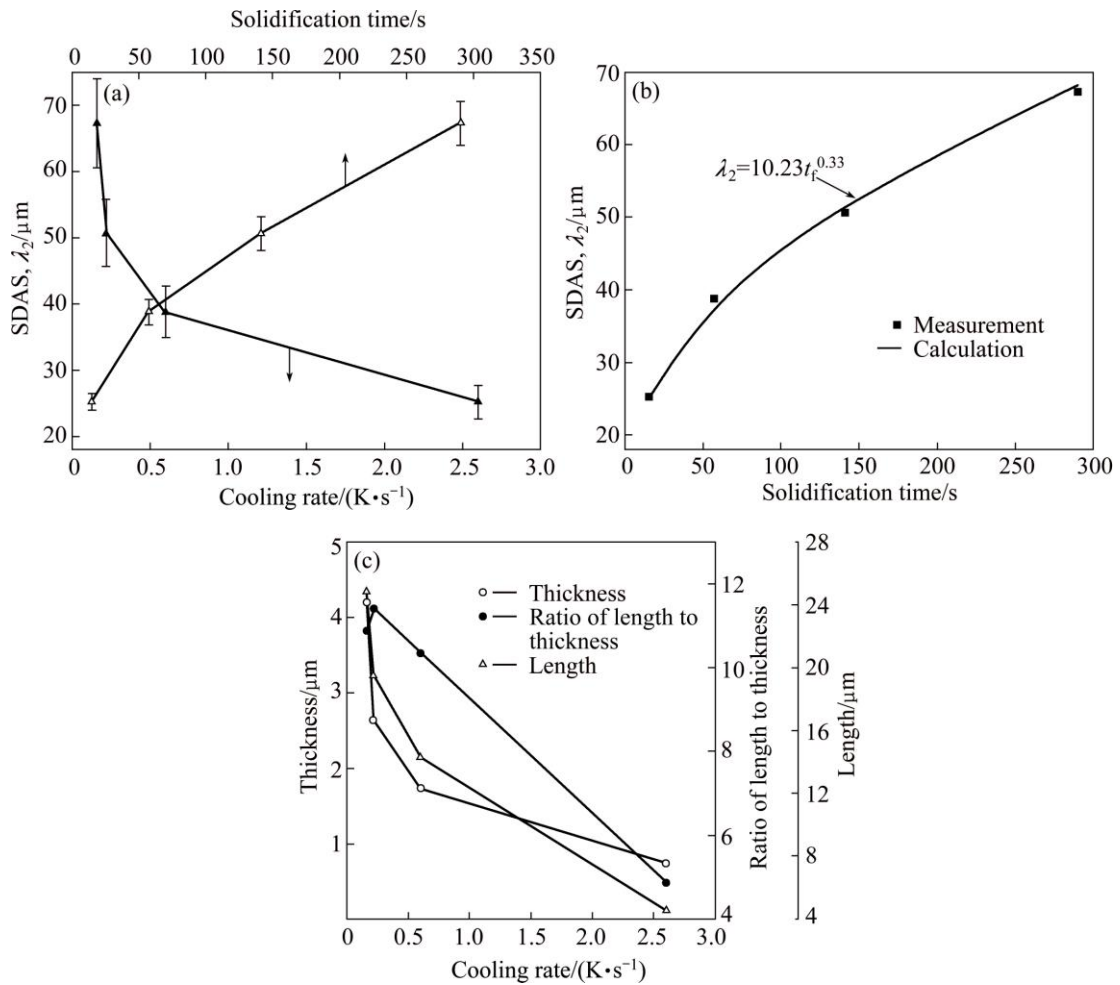

Fig. 6 Measured sizes of α(Al) and eutectic Si for A356 Al alloys: (a) SDAS plotted against cooling rates and solidification time; (b) Comparison of SDAS between experiment data and calculated results from equation $\lambda_2 = 10.23 t_f^{0.33}$ with λ_2 as secondary dendrite arm spacing and t_f as solidification time; (c) Measured shape-factor parameters of eutectic Si as function of cooling rates

of solidification time, as a good agreement between the calculative and experimental results is shown in Fig. 6(b). In order to precisely describe the morphology of eutectic Si, shape-factor parameters, such as the length, the width and the ratio of length to width of eutectic Si, as a function of cooling rate, were measured, as shown in Fig. 6(c). It is found that with increasing the cooling rate from 0.12 to 2.6 K/s, the values of the length, the width and the ratio of length to width of eutectic Si decrease from ~24.8 to ~4.53 μm, ~4.2 to ~0.75 μm and 10.8 to 4.8, respectively. One can see that with increasing the cooling rate, the eutectic Si tends to be of short-rod shape, even of spherical shape.

In addition, the transformed fraction of Al−Si eutectic phase was calculated by Newton thermal analysis (NTA) [16]. The evolution of solid transformed fraction $\varphi_s(T)$ during solidification was calculated based on the cooling curve, as shown in Fig. 7, where, $\varphi_s(T)$ is composed of two parts: the primary phase fraction, $\varphi_{Al}(T)$, and the Al−Si eutectic fraction, $\varphi_e(T)$, which are identified by a remarkable inflexion appearing at ~568 ℃ positioned by a vertical dash line. At cooling rate of 2.6 K/s, however, the inflexion occurs much beyond the Al−Si eutectic temperature (Fig. 7) due to an unremarkable plateau duration for Al−Si eutectic transformation (Fig. 3). With an assumption of $\varphi_{Al}(T)+\varphi_e(T)=1$, reducing the cooling rate can lead to a decrease of $\varphi_{Al}(T)$, and consequently an increase of $\varphi_e(T)$ (Fig. 7). Therefore, the high $\varphi_{Al}(T)$ due to high cooling rate restricts the dendrite coarsening, thus reducing the SDAS and consequently changing eutectic Si morphologies from coarse plate-like to short-rod shape even spherical shape because Al−Si eutectic usually forms within the interdendritic space.
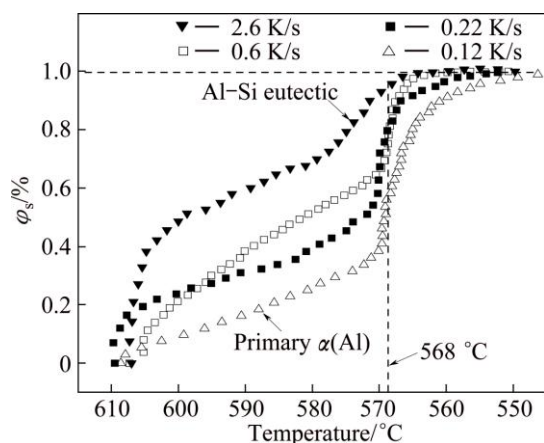

Fig. 7 Calculated results of solid transformed fraction vs temperature of A356 Al alloys by NTA at different cooling rates

3.4 Characteristics of as-cast microstructure after T4 treatment

After T4 treatment, the microstructures of as-cast samples are shown in Fig. 8. Compared with Fig. 7, the

eutectic Si is clearly modified and its modification degree depends on the cooling rate. For instance, eutectic Si is efficiently spheroidized at R=2.6 K/s (Fig. 8(a)), partially spheroidized and fragments at R=0.6 K/s (Fig. 8(b)), and only edge-rounded at R=0.22 K/s and R=0.12 K/s (Figs. 8(c) and (d)). This suggests that under the same solution treatment condition, the eutectic Si modified by increasing the cooling rate is more readily modified. In addition, except for α(Al) phase, Si phase and a little Fe-containing intermetallic phase, Mg_2Si phase is not examined by EDS, implying that annealing at 540 ℃ for 1 h is sufficient for the dissolution of coarse Mg_2Si produced in solidification into the Al matrix, meeting to the results from Ref. [3], as well as for a good modification of eutectic Si solidified at higher cooling rate, e.g., R=2.6 K/s.

3.5 Microhardness evolution before and after T4 treatment process

Figure 9(a) shows the microhardness evolution of primary α(Al) and eutectic Si phase as a function of cooling rate. As can be seen that with decreasing the cooling rate from 2.6 to 0.12 K/s, the microhardness of both α(Al) and eutectic Si phase reduces slightly. The microhardness of HV 84 and HV 101 of α(Al) and eutectic phase, respectively, is achieved at R=2.6 K/s, much larger than that of other samples. Subjected to T4 treatment, the microhardness of both primary α(Al) and Al−Si eutectic phase is shown in Fig. 9(b). By comparing with Fig. 9(a), the microhardness subjected to T4 heat treatment is much higher than that not subjected to T4 heat treatment. Interestingly, the maximum microhardness (HV 98 and HV 118 corresponding to α(Al) and Al−Si eutectic phase, respectively) is still achieved on the sample cast at R=2.6 K/s.

4 Discussion

4.1 Effects of cooling rate on solidification microstructure

In Section 3.3, the microstructure evolution is significantly dependent on the cooling rate. As shown in Fig. 6(a), the precise relationship between the SDAS, λ_2, and the cooling rate, R, can be described by Eq. (1) (Fig. 6(b)) based on an assumption that R is inversely proportional to the solidification time, t_f, and the similar results were reported in Ref. [17]. Clearly, the SDAS is significantly refined by increasing the cooling rate, and the fine SDAS can contribute to an improvement of microhardness of A356 Al alloy (Fig. 9(a)) due to more grain boundaries to hinder dislocation movement [18]. In addition, the increased volume fraction of primary α(Al) with increasing the cooling rate (Fig. 7) can lead to: 1) the modified eutectic Si morphology changing from
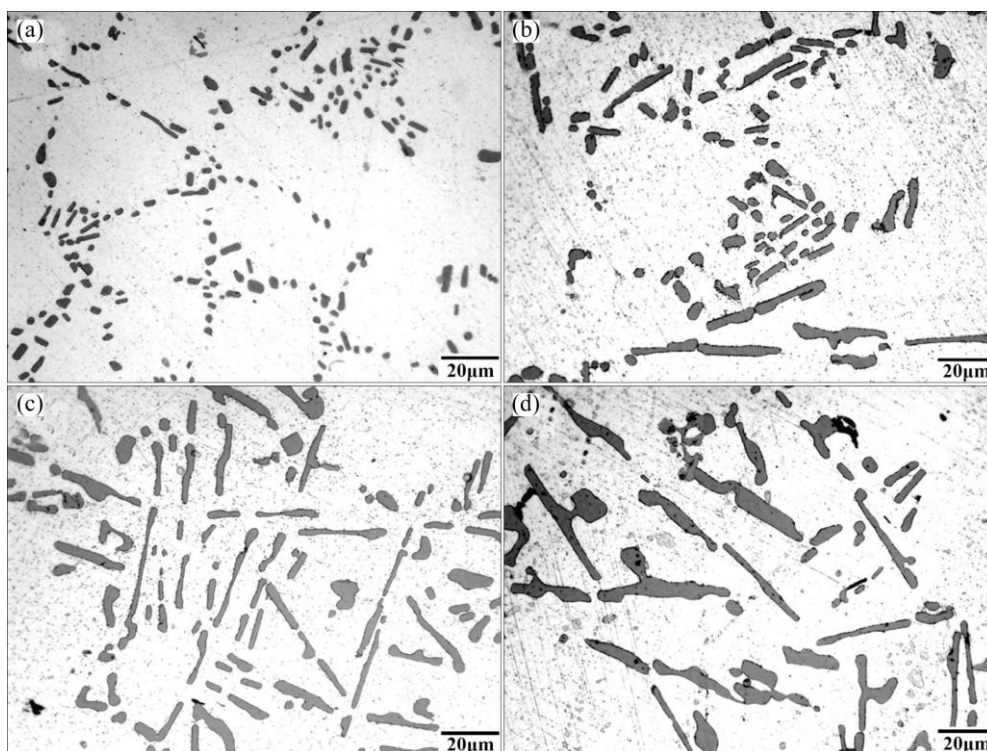
Fig. 8 Eutectic Si morphologies of A356 Al alloys subjected to T4 treatment and cast at 2.6 K/s (a), 0.6 K/s (b), 0.22 K/s (c) and 0.12 K/s (d)
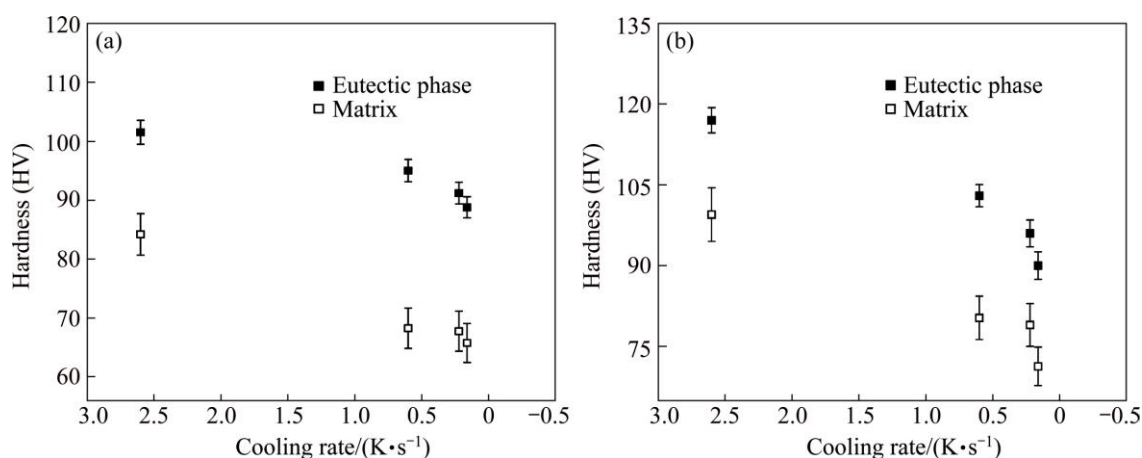

Fig. 9 Microhardness of A356 Al alloy vs cooling rate at cast state (a) and after T4 treatment (b)

coarse plate-like to short-rod shape (Figs. 5 and 6(c)) due to the small interdendritic spacing of primary α(Al) to restrict the nucleation and growth of Al−Si, namely as known "quenching modification", by which the Al−Si eutectic is hardened (Fig. 9(a)); 2) less volume fraction of Al−Si eutectic due to the coupled growth manner upon Al−Si eutectic transformation, and the similar results were reported in Ref. [19] which calculated the volume faction of transformed phase according to baseline method applied on cooling curve.

On the other hand, the solid solubility of Si and Mg atoms in the Al matrix is enhanced by increasing the cooling rate. The EDS shows that the solubility of Si

atom in the Al matrix at room temperature is ~1.32% (mole fraction) (much larger than the equilibrium value of 0.06%) at R=2.6 K/s. Therefore, the lattice parameter of Al_{fcc} matrix is significantly influenced (Fig. 4), thus the microhardness of primary α(Al) is improved due to its lattice distortion. This effect is thus named as solid-solution strength [20]. Moreover, the more supersaturated Si and Mg atoms in the Al matrix with increasing the cooling rate can significantly reduce the content of Fe-containing intermetallic, e.g., Al_5FeSi (Fig. 5), and $Al+Mg_2Si+Si$ ternary eutectic (Fig. 2) in lack of sufficient free Mg and Si atoms to supply their transformation, as a result, both the tensile strengthen

and elongation of alloys are improved to some extent [21].

Finally, it is valuable and necessary to stress the positive effect of post-solidification heat on the modification of eutectic Si. As shown in Fig. 3, the cooling curves in the post-solidification stage shows the low temperature drop in the temperature range of 350−567 ℃, implying that the solidification heat is not released as quickly as possible to the surrounding environment, thus the post-solidification heat is defined herein. In theory, this post-solidification heat can lead to the slight modification for eutectic Si due to the widely known "thermal modification" [22], especially for the refined eutectic Si (the detail will be shown in Section 4.2). This hypothesis was confirmed by the experiment results. For instance, Fig. 5(a) shows that the edges of eutectic Si at R=2.6 K/s are slightly rounded, but the samples at R=0.6, 0.22 and 0.12 K/s are not (Figs. 5(b)−(d)). Two reliable reasons can be interpreted: 1) the samples at R=2.6 K/s suffer more effect of post-solidification heat, e.g., in the temperature range of 350−540 ℃ for ~10 min, than others; 2) the refined as-cast microstructure can accelerate eutectic Si modification process (see Section 4.2). On this basis, if the post-solidification heat is used efficiently, the solution treatment procedure will be shrunk, even abolished. The preliminary relevant investigation has been reported in Ref. [23]. Therefore, the further investigation on the post-solidification heat effect should be performed in future for a minimum product cost, especially in the sand casting process.

In conclusion, the size, morphologies and volume fraction of solidification microstructure are significantly dependent on the cooling rate. The special microstructures, such as small SDAS, fine Al−Si eutectic, a few of Fe-containing phases, Al+Si+Mg$_2$Si brittle phase and high solubility of Mg and Si in the Al matrix due to the increased cooling rate, not only can lead to the maximum hardness but are beneficial to the subsequent solution treatment (see Section 4.2).

4.2 Modification of eutectic Si in solution treatment

To gain the significant mechanical properties especially the ductility of Al−Si−Mg alloys, eutectic Si is usually modified from flake-like to the fibrous or spherical shape by three ways [24]: chemical, quenching and thermal modifications.

As discussed in Section 4.1, eutectic Si presents different modifications due to different cooling rates, i.e., quenching modification. Subjected to the same T4 treatment, the finer Si is more readily and sufficiently spheroidized than the coarser one (Fig. 8), implying that eutectic Si subjected to the pre-modification, e.g., quenching modification in the solidification process,

gives faster response of thermal modification. In fact, the thermal modification of eutectic Si contains three stages: edges rounding (Fig. 10(a)), bays occurring (Fig. 10(b)) and fragmentation followed by spheroidization (Fig. 10(c)), and the same investigation was reported elsewhere [25]. The EDS is used to describe the thermal modification process and indicates that the concentration fluctuation of eutectic Si along its length direction (Fig. 10(a)) leads to a "bays", which stretches from the periphery into the plate with prolonging the solution time (Fig. 10(b)). With further prolonging the solution time, these bays become deep and finally fragment
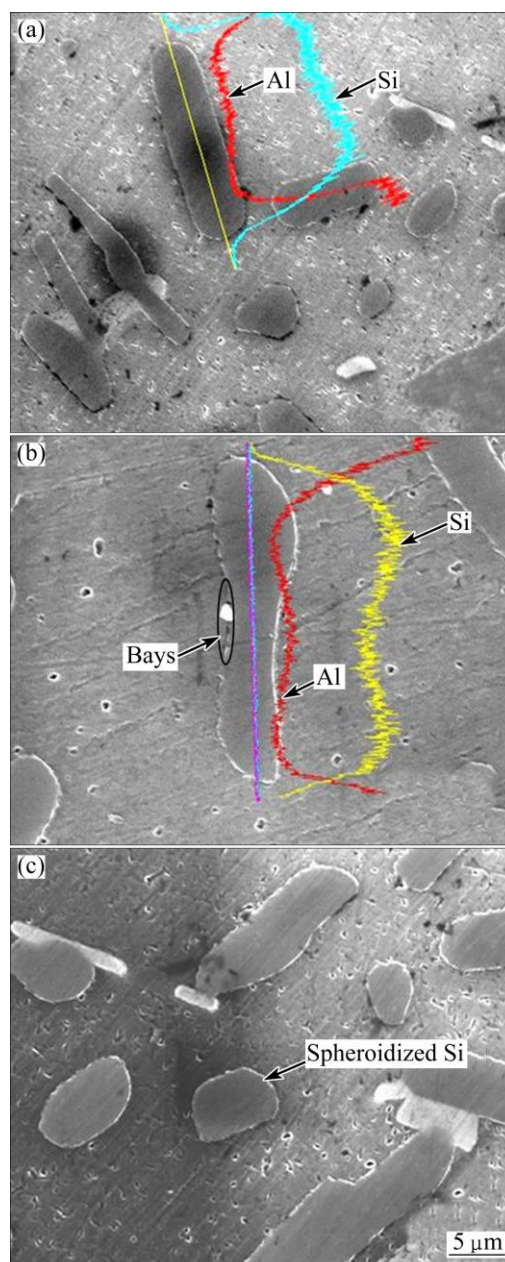

Fig. 10 Morphologies (SEM) and concentrations (EDS) of eutectic Si subjected to T4 treatment showing three stages of its modification: (a) Edges rounding; (b) Bays occurring; (c) Fragmentation and spheroidization

(Fig. 10(c)), thus a whole spheroidization process is finished. One can see that the spheroidization of Si substantially is a process related to the diffusion and dissolution of Si atoms. Due to much smaller activation energy (~1.4 eV [26]) of Al−Si inter-diffusion compared with that (~2.3 eV [27]) of Si surface self-diffusion, the inter-diffusion is regarded as more probable mechanism of Si diffusion. As for Si particle dissolution, an approximate calculation of dissolution time can be performed by the following equation [28]:

$$\frac{\mathrm{d}R}{\mathrm{d}t} = -\Omega \left[\frac{D}{R_0} + \sqrt{\frac{D}{\pi t}} \right] \tag{2}$$

where R_0 is the initial particle size, Ω is the super-saturation and D is the diffusion coefficient. Obviously, both small R_0 and large Ω can increase the value of $\mathrm{d}R/\mathrm{d}t$, i.e., reducing the dissolution time. Consequently, the fact that eutectic Si subjected to higher cooling rate is more readily modified under T4 treatment condition is due to refined eutectic Si and large solubility of Si in the Al matrix. Moreover, because of the inter-diffusion mechanism for eutectic Si modification, the small SDAS is also inferred to aid reducing the solution time due to small diffusion distance between Si and α(Al).

According to Ref. [29], the modified eutectic Si after T4 treatment makes the microhardness of alloy improve significantly. Meanwhile, according to Ref. [30], natural aging for 24 h is another factor to improve the microhardness of A356 Al alloy due to the formation of solution clusters. As a result, the microhardness value in Fig. 9(b) is larger than that in Fig. 9(a). In addition, subjected to the same T4 treatment, the maximum hardness is achieved on the sample cast at R=2.6 K/s (Fig. 9). This is ascribed to more sufficiently modified eutectic Si and more amount of solution cluster [31].

In summary, the optimal combination of solidification parameters, i.e., cooling rate, with heat treatment process may achieve the minimum product cost but a better modification of eutectic Si.

5 Conclusions

1) The end-chilled sand casting method was used for the casting process of commercial A356 Al alloy. The different solidification microstructures with cooling rates of 2.6, 0.6, 0.22 and 0.12 K/s were obtained.

2) With the increase of cooling rate, the SDAS is reduced; eutectic Si is modified from coarse plate-like to short-rod shape even to spherical shape; the Al+Si+Mg$_2$Si ternary eutectic transformation is restarted and the dissolubility of enriched Mg- and Si-clusters in α(Al) is enhanced. All of these typical microstructures result in an improved microhardness.

3) Subjected to the T4 treatment, eutectic Si cast at higher cooling rate is more readily spheroidized than that at lower cooling rate, whilst the corresponding microhardness is also achieved the maximum value at high cooling rate. This suggests that an optimal combination of solidification path and heat treatment may achieve a better mechanical property but a minimum product cost.

References

[1]   ESTEY C M, COCKCROFT S L, MAIJER D M, HERMESMANN C. Constitutive behaviour of A356 during the quenching operation [J]. Materials Science and Engineering A, 2004, 383: 245−251.

[2]   DIONI D, CECCHEL S, CORNACCHLA G, FACCOLI M, PANVINI A. Effects of artificial aging conditions on mechanical properties of gravity cast B356 aluminum alloy [J]. Transactions of Nonferrous Metals Society of China, 2015, 25(4): 1035−1042.

[3]   LADOS D A, APELIAN D, WANG L B. Solution treatment effects on microstructure and mechanical properties of Al−(1 to 13 pct) Si−Mg cast alloys [J]. Metallurgical and Materials Transactions B, 2011, 42(1): 171−180.

[4]   MARTINEZ E J, CISNEROS M A, VALTIERRA G S, JACAZE J. Effect of strontium and cooling rate upon eutectic temperatures of A319 aluminum alloy [J]. Scripta Materialia, 2005, 52: 439−443.

[5]   ZHU M, JIAN Z Y, YAO L J, LIU C X, YANG G C, ZHOU Y H. Effect of mischmetal modification treatment on the microstructure, tensile properties, and fracture behavior of Al−7.0%Si−0.3%Mg foundry aluminum alloys [J]. Journal of Materials Science, 2011, 46(8): 2685−2694.

[6]   EL SEBAIE O, SAMUEL A M, SAMUEL F H, DOTY H W. The effects of mischmetal, cooling rate and heat treatment on the hardness of A319.1, A356.2 and A413.1 Al–Si casting alloys [J]. Materials Science and Engineering A, 2008, 486: 241−252.

[7]   LIU R P, HERLACH D M, VANDYOUSSEFI M, GREER A L. Morphologies of silicon crystals solidified on a chill plate [J]. Metallurgical and Materials Transactions A, 2004, 35(3): 1067−1073.

[8]   ZHANG L Y, JIANG Y H, MA Z, SHAN S F, JIA Y Z, FAN C Z, WANG W K. Effect of cooling rate on solidified microstructure and mechanical properties of aluminium-A356 alloy [J]. Journal of Materials Processing Technology, 2008, 207: 107−111.

[9]   CHEN Z W, JIE W Q, ZHANG R J. Superheat treatment of Al−7Si−0.55Mg alloy melt [J]. Materials Letters, 2005, 59: 2183−2185.

[10]   XU C L, JIANG Q C. Morphologies of primary silicon in hypereutectic Al−Si alloys with melt overheating temperature and cooling rate [J]. Materials Science and Engineering A, 2006, 437: 451−455.

[11]   WANG Q G, DAVIDSON C J. Solidification and precipitation behaviour of Al−Si−Mg casting alloys [J]. Journal of Materials Science, 2001, 36(3): 739−750.

[12]   WANG H P, YAO W J, WEI B. Remarkable solute trapping within rapidly growing dendrites [J]. Applied Physics Letters, 2006, 89: 201−205.

[13]   MÖLLER H, GOVENDER G, STUMPF W E, PISTORIUS P C. Comparison of heat treatment response of semisolid metal processed alloys A356 and F357 [J]. International Journal of Cast Metals Research, 2010, 23: 37−43.

[14]   MARTINEZ R A, FLEMINGS M C. Evolution of particle morphology in semisolid processing [J]. Metallurgical and Materials Transactions A, 2005, 36(8): 2205−2210.

[15] EASTON M A, DAVIDSON C A, STJOHN D A. Effect of alloy composition on the dendrite arm spacing of multicomponent aluminum alloys [J]. Metallurgical and Materials Transactions A, 2010, 41(6): 1528−1538.

[16] CRUZ H, GONZALEZ C, JUAREZ A, HERRERA M, JUAREZ J. Quantification of the microconstituents formed during solidification by the Newton thermal analysis method [J]. Journal of Materials Processing Technology, 2006, 178: 123−134.

[17] MARTINEZ R A, FLEMINGS M C. Evolution of particle morphology in semisolid processing [J]. Metallurgical and Materials Transactions A, 2005, 36(8): 2205−2210.

[18] HANSEN N. Hall-Petch relation and boundary strengthening [J]. Scripta Materialia, 2004, 51: 801−806.

[19] XU J F, LIU F. Baseline method for determining the solid fraction [J]. Advances in Materials Research, 2012, 562−564(5): 409−413.

[20] CACERES C H, ROVERA D M. Solid solution strengthening in concentrated Mg−Al alloys [J]. Journal of Light Metals, 2001, 1(3): 151−156.

[21] ZHU M, JIAN Z Y, YANG G C, ZHOU Y H. Effects of T6 heat treatment on the microstructure, tensile properties, and fracture behavior of the modified A356 alloys [J]. Materials and Design, 2012, 36: 243−249.

[22] SATHYAPAL H, NARAYAN PRABHU K. Modification of eutectic silicon in Al−Si alloys [J]. Journal of Materials Science, 2008, 43(9): 3009−3027.

[23] CHEN X, KASPRZAK W, SOKOLOWSKI J H. Reduction of the heat treatment process for Al-based alloys by utilization of heat from the solidification process [J]. Journal of Materials Processing Technology, 2006, 176: 24−31.

[24] JIAN X, MEEK T T, HAN Q. Refinement of eutectic silicon phase of aluminum A356 alloy using high-intensity ultrasonic vibration [J]. Scripta Materialia, 2006, 54: 893−896.

[25] YAMAGATA H, KASPRZAK W, ANIOLEK M, KURITA H, SOKOLOWSKI J H. The effect of average cooling rates on the microstructure of the Al−20%Si high pressure die casting alloy used for monolithic cylinder blocks [J]. Journal of Materials Processing Technology, 2008, 203: 333−341.

[26] FUJIKAWA S I, HIRANO K I, FUKUSHIMA Y. Diffusion of silicon in aluminum [J]. Metallurgical and Materials Transactions A, 1978, 9(12): 1811−1815.

[27] KEFFE M E, UMBACH C C, BLAKELY J M. Surface self-diffusion on Si from the evolution of periodic atomic step arrays [J]. Journal of Physics and Chemistry of Solids, 1994, 55: 965−973.

[28] AARON H D, KOTLER G R. Second phase dissolution [J]. Metallurgical and Materials Transactions B, 1971, 2(2): 393−408.

[29] XU C L, YANG Y F, WANG H Y, JIANG Q C. Effects of modification and heat-treatment on the abrasive wear behavior of hypereutectic Al−Si alloys [J]. Journal of Materials Science, 2007, 42(15): 6331−6338.

[30] SHA G, MLLER H, STUMPF W E, XIA J H, GOVENDER G, RINGER S P. Solute nanostructures and their strengthening effects in Al−7Si−0.6Mg alloy F357 [J]. Acta Materialia, 2012, 60: 692−701.

[31] DANG B, LI Y B, LIU F, ZUO Q, LIU M C. Effect of T4 heat treatment on microstructure and hardness of A356 alloy refined by Ga+ In+ Sn mixed alloy [J]. Materials and Design, 2014, 57: 73−78.

A356 铝合金的凝固组织特征对固溶处理工艺的影响

党 波，刘丛丛，刘 峰，刘颖卓，李远兵

西北工业大学 凝固技术国家重点实验室，西安 710072

摘 要：为了提高性能且降低成本，设计末端激冷的砂型铸造实验，研究 A356 铝合金的凝固组织随冷却速率的演化特征以及不同凝固组织对后续固溶处理过程的影响。实验结果表明：初生相 α(Al)的二次枝晶间距、共晶 Si 的尺寸以及 Al−Si 共晶体积分数随冷却速率的提高而减小。经过 540 ℃ 固溶处理 1 h 后淬火，当冷却速率为 2.6 K/s 时，共晶 Si 完全球化；当冷却速率为 0.22 K/s 时，共晶 Si 发生部分球化；当冷却速率为 0.22 和 0.12 K/s 时，仅共晶 Si 的边缘发生钝化。同时，当冷却速率为 2.6 K/s 时，合金具有最大的显微硬度。由此可见，经过高冷却速率凝固后，细化的共晶 Si 更容易发生球化，从而在给定固溶温度条件下，降低了固溶处理所需要的时间，即降低了生产成本。

关键词：A356 铝合金；固溶处理；冷却速率；共晶 Si；变质处理

(Edited by Mu-lan QIN)